INL/CON-11-22073
PREPRINT

Thermal Predictions of New Composite Material During Inpile Testing

NURETH-14

Donna Post Guillen
W. David Swank
Adam X. Zabriskie
Heng Ban

September 2011

The INL is a
U.S. Department of Energy
National Laboratory
operated by
Battelle Energy Alliance

The 14th International Topical Meeting on Nuclear Reactor Thermal Hydraulics, NURETH-14
Toronto, Ontario, Canada, September 25-29, 2011

NURETH14-108

THERMAL PREDICTIONS OF NEW COMPOSITE MATERIAL DURING INPILE TESTING

Donna Post Guillen,[1] W. David Swank,[1] Adam X. Zabriskie[2] and Heng Ban[2]
[1]Idaho National Laboratory, Idaho Falls, ID USA
[2]Utah State University, Logan, UT USA
Donna.Guillen@inl.gov, W.Swank@inl.gov, xenon54z@gmail.com, heng.ban@usu.edu

Abstract

An inpile experiment is currently underway wherein specimens comprised of a newly developed material are being irradiated at Idaho National Laboratory's Advanced Test Reactor (ATR) in conjunction with Utah State University under the auspices of the ATR National Scientific User Facility. This paper provides the thermophysical properties of this new material measured prior to irradiation. After the irradiation campaign is complete, the thermophysical properties of the specimens will be measured and compared to the preirradiation values. A finite-element model was constructed to predict bounding specimen temperatures during irradiation. Results from the thermal hydraulic modeling, including the steady-state temperatures of the specimens within sealed capsules, are presented. After the irradiation campaign is completed, best-estimate thermal predictions will be performed for the individual specimens using the actual as-run irradiation power levels.

Keywords: Thermal hydraulics, irradiation experiment, finite element analysis

Introduction

Idaho National Laboratory (INL) is developing a new material to enable the development of a system with the capability to conduct fast neutron irradiation testing in the Advanced Test Reactor (ATR). The Boosted Fast Flux Loop (BFFL), derived from the Gas Test Loop, is a concept designed to provide fast flux test capability by using one of the ATR corner lobes with the addition of a thermal neutron filter to absorb the thermal neutrons and booster fuel to augment the neutron flux. An absorber material comprised of hafnium aluminide (Al_3Hf) particles in an aluminum matrix (Al_3Hf-Al) can absorb thermal neutrons and transfer heat from the experiment to pressurized water cooling channels. The source of neutrons provided by the ATR driver fuel comprises fast neutrons and thermal neutrons, with the neutron absorber absorbing some of the thermal neutrons. The resulting fast neutron flux, averaged over the central 40 cm relative to ATR core midplane experienced by the irradiation positions, would be ~1.04×10^{15} n/cm^2-s with a fast-to-thermal flux ratio in excess of 20 [1].

Thermal analyses conducted on a candidate configuration confirmed that the design of the water-cooled Al_3Hf-Al absorber block is capable of maintaining all system components below their maximum allowable temperature limits [2]. However, the thermophysical properties of Al_3Hf, such as thermal conductivity, have never been measured, and the effect of irradiation on

these properties has never been determined. The radiation effects that are commonly associated with intermetallic phases are amorphization and increased or decreased phase stability [3],[4]. In the preliminary assessment, the mechanical and chemical properties of Al_3Hf were similar to previously studied Al_3Zr, and the thermal conductivity of Al_3Hf was estimated based on UAl_4, which has similar phase transition. It is essential for the development of the BFFL to obtain data on the effect of irradiation on the thermophysical and mechanical properties of the Al_3Hf intermetallic and Al_3Hf-Al metal matrix composite. Other information, such as corrosion behavior and radioactive decay products, are also necessary to proceed with the design and optimization of the BFFL system.

A drop-in experiment is currently underway wherein material specimens are being irradiated in conjunction with Utah State University under the auspices of Idaho National Laboratory's Advanced Test Reactor National Scientific User Facility [5]. The thermophysical and mechanical properties of the Al_3Hf intermetallic and the Al_3Hf-Al composite material were measured prior to and will be measured after irradiation. This paper provides the thermophysical properties of this new material measured prior to irradiation. After the irradiation campaign is complete, the thermophysical properties of the specimens will be measured and compared to the preirradiation values. Since thermal neutron flux varies with axial position within the core, the various specimens will be subjected to different heat loads (and temperatures). A finite-element model of the experiment assembly was constructed to predict bounding specimen temperatures during a nominal irradiation cycle. Results from the thermal hydraulic modeling, including the steady-state temperatures of the specimens within static capsules, are presented.

1. Experiment description

The experiment is designed to be housed in a small B position (B2) located in the eastern section of the ATR. The irradiation test assembly consists of a basket and three drop-in capsule pairs containing the material specimens. The capsule pairs contain various size specimens of Al_3Hf intermetallic (100 vol%) and Al_3Hf-Al composite material fabricated with three different Al_3Hf volume percentages (20.0, 28.4, and 36.5 vol%). Neutronic calculations have shown that ~7 at% of Al_3Hf in an aluminum matrix yields the optimum fast flux and fast-to-thermal ratios [6]. This atomic percentage corresponds to a 28.4 vol% Al_3Hf. Composite material with higher and lower volume percentages of intermetallic in the aluminum matrix were incorporated into the experiment to explore the effects of radiation-induced changes to the material.

The capsule pairs consist of a top and a bottom capsule. The bottom capsule is inverted 180 degrees from the orientation of the top capsule. For each reactor cycle, three capsule pairs are housed in a basket. The basket serves to position the capsules within the irradiation position, allows adequate coolant circulation to prevent temperature distortions or adverse mechanical effects, and provides adequate structural support for the capsule pairs during reactor insertion, irradiation, and removal from the reactor. The capsules provide a robust barrier between the water coolant and the material specimens. The capsule assemblies are backfilled with helium gas to enhance heat transfer from the specimens. All test assembly components (except for the specimens) are constructed from Aluminum 6061 alloy.

Flux wire monitors located within the capsules are used to quantify the neutron flux at designated locations in the irradiation test assembly. The flux wire monitors are incorporated into the capsule pairs as follows:

- One monitor per capsule pair to calibrate the Monte Carlo Neutron Particle (MCNP) neutronics code calculations. Aluminum alloy holders (1 × 1 cm cylinder) surround the flux wire monitors located in the top capsule of the capsule pair.
- One monitor per capsule pair to assess the neutron flux perturbation by the material. Holders (1 × 1 cm cylinder) fabricated from 28.4 vol% composite material surround the flux wire monitors located in the bottom capsule (Assembly 2) of the capsule pair.

The specimens contained in the capsules were machined into various specimen geometries from six billets of hot-pressed metal matrix composite material and castings of intermetallic material. The four different specimen geometries (shown in Figure 1) are:

- Rods 5 mm in diameter × 5 mm long, fabricated from either Al_3Hf intermetallic or Al_3Hf-Al composite material
- Disks 5 mm in diameter × 0.8 mm thick, fabricated from Al_3Hf-Al composite material
- Disks 3 mm in diameter × 0.3 mm thick, fabricated from Al_3Hf-Al composite material
- Dogbone-shaped tensile specimens 16 × 4 × 1 mm, fabricated from Al_3Hf-Al composite material.

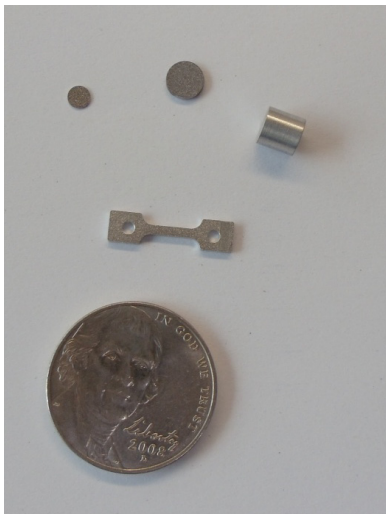

Figure 1 Specimen geometries.

Because of the brittle nature of the material, it was not possible to machine very thin specimens from intermetallic (100 vol%) material. Machining tolerances are within ±0.05 mm.

2. Model development

The irradiation experiment configured by Utah State University (USU) was modeled using ABAQUS CAE [7] for construction of the finite element model and ABAQUS Standard to calculate steady-state and transient temperatures and heat fluxes. The finite element model geometry was constructed using three-dimensional solid elements. The eight-node linear brick element (DC3D8) was used to model the reflector, basket, and capsule pairs. The ATR primary coolant water flowing between the capsules and the basket, and between the basket and the reflector, was modeled using an eight-node convection-diffusion brick element (DCC3D8).

Because of the uncertain change in thermophysical properties with irradiation, a bounding approach was employed for the thermal analysis to determine the highest temperatures the specimens could reach and ensure the safety of the irradiation test assembly. The capsule geometry was simplified and worst-case thermophysical properties applied.

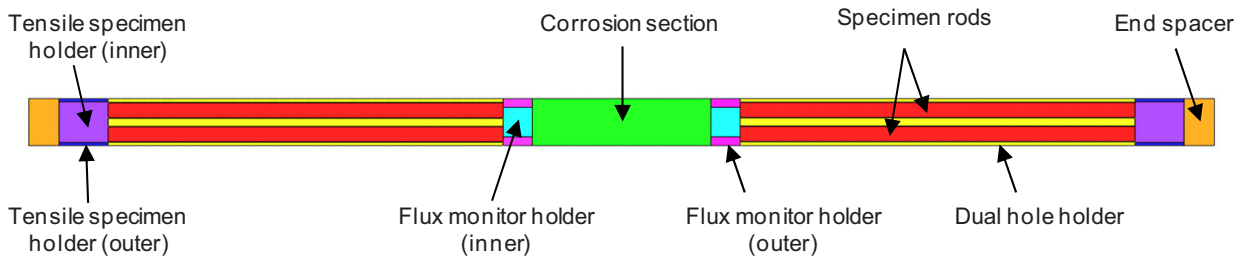

Figure 2 Part instances in one capsule pair.

Each capsule in the model is comprised of five sections. These sections are illustrated in Figure 2 and the various part instances are color-coded as described below.

1. End spacer [*orange*] – Solid Aluminum 6061 end cap.

2. Tensile specimen holder – This section is modeled with an inner part (tensile-holder-inner [*purple*]) consisting of a section representing the tensile specimens housed in an Aluminum 6061 holder. This inner holder is surrounded by an Aluminum 6061 tube (tensile-holder-outer [*dark blue*]) and separated by a helium gas gap. The geometry of the tensile specimens is approximated because of difficulties obtaining a converged solution with the complex geometry of the dogbone-shaped specimens and corresponding holder. The entire section containing the tensile specimens was assigned material properties corresponding to 36.5 vol% Al_3Hf-Al composite and a heat load corresponding to the hottest tensile specimen from the MCNP analysis.

3. Main holder consisting of a dual-hole holder [*yellow*] and two specimen rods [*red*] – The dual-hole holder is essentially an Aluminum 6061 rod with two longitudinal holes bored through its length. In each hole, disk- and/or rod-shaped specimens are separated by Aluminum 6061 spacers and stacked axially. Rather than modeling all 32 specimens per capsule pair contained in these holes, the individual specimens and spacers are considered to be a solid rod. Each rod is separated from the holder by a helium gas gap. A slot filled with helium gas connects the two holes. The cylindrical specimen stacks are modeled as solid rods comprised of 36.5 vol% Al_3Hf-Al composite. Each stack is partitioned into three axial sections and an average heat load provided by an MCNP physics analysis is applied to each section.

4. Flux monitor holder – This section is modeled as an inner part consisting of the flux monitor holder (flux-monitor-holder-inner [*turquoise*]) that fits into an Aluminum 6061 outer tube (flux-monitor-holder-outer [*fuchsia*]). These two parts are separated by a helium gas gap. The flux monitor holder is assumed to be a solid cylinder of solid Aluminum 6061 for the top capsule and 28.4 vol% Al_3Hf-Al composite for the bottom capsule.

5. Corrosion section [*green*] – The experiment was originally designed to include a flow-through section with corrosion specimens. This feature was eliminated and replaced with a solid aluminum section located between the top and bottom capsule pair.

The separate parts are instanced into the assembly and connected axially by tie constraints to enable heat conduction within the capsules. Figure 3 illustrates the finite element mesh used for the various components. The capsule pairs are stacked axially within the basket and are designated downward from the reactor top as A, B, and C in the ABAQUS model, with A being the *upper* capsule pair, B the *middle* capsule pair, and C the *lower* capsule pair. The top capsule of each pair is designated in the drawings as Assembly 1; whereas, the bottom capsule of each capsule pair is designated as Assembly 2. The capsules are surrounded by an inner water channel, basket, outer water channel, and reflector.

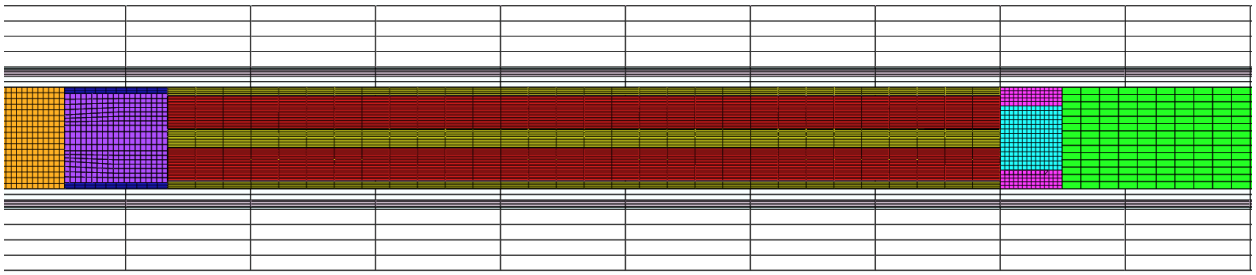

Figure 3 Finite element mesh detail of a single capsule.

3. Calculations and analysis

3.1 Thermal hydraulic analysis

The ATR is cooled by pressurized (2.5 MPa) water. Coolant flow enters the experiment assembly from the top of the reactor with an inlet temperature of 325 K. Flowing water travels downward through the test train in the channel between the basket and the capsules and in the channel between the basket and the beryllium reflector. The velocity of cooling water in the water channels was calculated using the extended Bernoulli equation using the inlet conditions and pressure drop (0.53 MPa) for two-pump operation. An 8% reduction in flow velocity was applied to the flow in the outer coolant channel to account for cross-flow effects from the saw cuts in the beryllium reflector. Heat flux from the reflector to the cooling water is taken into account by modeling the reflector as a 0.009525 m thick tube with an adiabatic boundary at the outer diameter.

The calculated flow rates are 5.096×10^{-4} m^3/s for the inner water channel and 2.363×10^{-4} m^3/s for the outer water channel. Heat transfer coefficients for turbulent forced convection to the cooling water were obtained from the Colburn correlation using the film temperature method to account for fluid property variation [8]. Forced convection heat transfer to the primary cooling water occurs in the channel between the capsules and the basket (denoted the inner channel) and between the basket and the reflector (denoted the outer channel). Contact surfaces for forced convection include the: (1) outside surface of capsules and inside surface of basket with primary coolant water in the inner channel, and (2) outside surface of the basket and inside surface of reflector with primary coolant water in the outer channel. The water thermal conductivity is artificially increased by several orders of magnitude in the perpendicular x- and y-directions to the flow to simulate mixing in the turbulent flow channels.

The heat loads for the experiment while in the reactor were obtained from an MCNP reactor physics analysis at approximately 24.3 MW(t) east lobe source power. To obtain volumetric heat rates, the heat loads in W/g were multiplied by the material density and input into the ABAQUS model in units of W/m^3. Heating of aluminum structural materials is mainly the result of gamma ray absorption. Heating of the water, hafnium aluminide materials, and beryllium reflector also include the effect of neutron heating. Heat loads for the reflector, basket, and water channels were provided as a function of distance from the core midplane to account for the axial variation in core power.

Heat transfer across gas gaps within the capsules are modeled using the gap conductance and gap radiation models. Gas gaps are present between the dual-hole holder and specimen rods, the slot in dual-hole holder, the inner and outer flux-monitor holders, and the inner and outer tensile holders. Heat transfer coefficients for conduction across gas gaps were calculated as a function of gap size and temperature. Contact surfaces for helium gap conduction are the respective inside surfaces and outside surfaces of components participating in the heat transfer. Thermal contact between adjacent components was modeled using a tie constraint.

3.2 Thermophysical properties

Temperature-dependent thermophysical properties of aluminum, beryllium, compressed water, and helium were obtained from Perry's Chemical Engineers' Handbook [9]. Properties of the new hafnium aluminide materials were measured at INL on Al_3Hf intermetallic (100 vol%) and Al_3Hf-Al metal matrix composite material with three different Al_3Hf volume percentages (20.0, 28.4, and 36.5 vol%). The measured properties of the unirradiated materials, which were used to predict specimen temperatures during the irradiation experiment, will be compared with post-irradiation characterization measurements. Knowledge of irradiation effects on the material properties is necessary for the effective design of an Al_3Hf-Al absorber block system.

Specific heat, shown in Figure 4, was measured using a commercially available differential scanning calorimeter (Netzsch DSC 404C) per ASTM E 1269-05 [10]. Error bars indicate the standard deviation of the average of three measurements made at a given temperature [11]. This test method consisted of heating a specimen 3 mm in diameter × 0.3 mm thick at a controlled rate in a controlled atmosphere of helium over a temperature range from 50 to 530°C, in steps of 10°C. The difference in heat flow into the specimen material and a reference material of sapphire is continuously monitored and recorded to determine the specific heat of the specimen material.

Density measurements were performed at room temperature using ASTM B 311-08 [12]. This method determines density using the Archimedes' principle wherein density (ρ) is calculated by the following relation

$$\rho = \frac{W_a}{W_a - W_f}\rho_f \tag{1}$$

where W_a is the weight of the material in air, W_f is the weight of the material in the fluid, and ρ_f is the density of the fluid.

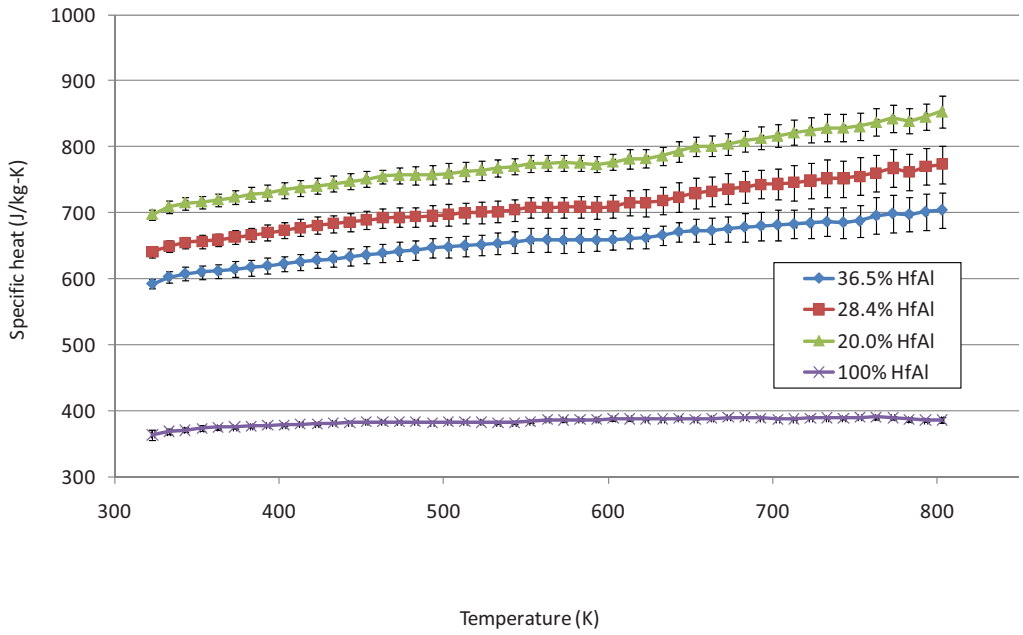

Figure 4 Specific heat of hafnium aluminide materials.

Density measurements were performed for six hot-pressed billets of composite material, providing two density measurements for each volume percent. Average values for density are provided in Table 1. Accompanying the density measurements that are important to thermophysical measurements, elemental chemical composition and qualitative x-ray diffraction analysis were also performed by an independent laboratory for quality assurance purposes.

Table 1 Density of material by volume percent.

Al_3Hf intermetallic (vol%)	Density (kg/m^3)
20	3400
28.4	3680
36.5	3960
100	6030

The ability to conduct heat through the filter material is critical to the passive removal of decay heat. Differences in thermal conductivity within the material can have a significant effect on the passive heat removal rate and thus the peak temperature that the filter will experience. Here, ASTM E 1461-07 [13] is followed for the calculation of thermal diffusivity and conductivity. Thermal diffusivity (α) is measured and defined as the ratio of thermal conductivity to volumetric heat capacity by

$$\alpha = \frac{k}{\rho c_p} \tag{1}$$

where k is the thermal conductivity and c_p is the specific heat.

The measurement of thermal diffusivity is performed on small, thin, disk-shaped specimens machined to 12 mm in diameter and 3 mm thick. A pulsed laser is used to subject one surface of the specimen to a high-intensity, short-duration energy pulse. The energy of this pulse is absorbed on the front surface of the specimen and the resulting rise in rear-face temperature is recorded. Thermal diffusivity is calculated from the specimen thickness and the time required for the rear face temperature to reach 50% of its maximum value. A commercially available laser flash apparatus (Netzsch LFA 457), complete with vendor-developed software for instrument control and data acquisition, was used. Measurements were made from room temperature to approximately 550°C, in steps of 50°C. Thermal conductivity, shown in Figure 5, was calculated from the measured values for thermal diffusivity, specific heat and density using Equation 1. Uncertainty in thermal conductivity was calculated by [14]

$$U_k = \sqrt{\left(\frac{\partial k}{\partial \alpha} U_\alpha\right)^2 + \left(\frac{\partial k}{\partial \rho} U_\rho\right)^2 + \left(\frac{\partial k}{\partial c_p} U_{c_p}\right)^2} \tag{2}$$

where U_α (m^2/s) is the uncertainty in thermal diffusivity (3% [15]), U_ρ (kg/m^3) is the uncertainty in density (0.5% [12]), and U_{cp} (J/kg-K) is uncertainty in specific heat (2.5% [16]).

Knowledge of the coefficient of thermal expansion (CTE) for filter components is critical for determining the dimensional changes that occur as a result of temperature cycles. Localized external stresses can be imposed upon mechanically interlocked composite particles as the individual pieces undergo differential thermal expansion. Internal stresses can occur if there is a temperature gradient causing differential expansion within the filter medium. Determining CTE values for different compositions allows a reliable prediction of stress states within filter components.

The CTE measured here follows ASTM E 228-06 [17]. This test method uses a commercial push-rod type dilatometer (Netzsch DIL 402C) to determine the change in length of a specimen as a function of temperature. The temperature is varied over the desired range at a slow constant heating or cooling rate. The linear thermal expansion and mean CTE, are calculated from the recorded data using

$$CTE = \frac{1}{L_0}\frac{\Delta L}{\Delta T} \tag{3}$$

where L_0 is the specimen initial length, ΔL is the change in length, and ΔT is the temperature difference between a specified reference temperature and the temperature at which the change in length was measured. Measurements were made from 100 to 520°C, in steps of 10°C. Variation of CTE with temperature are shown in Figure 6.

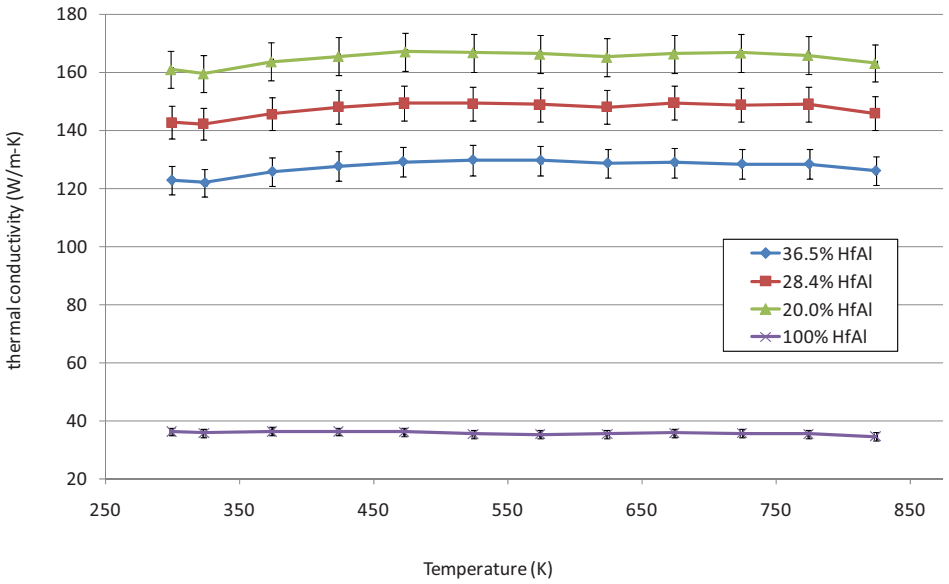

Figure 5 Thermal conductivity of hafnium aluminide materials.

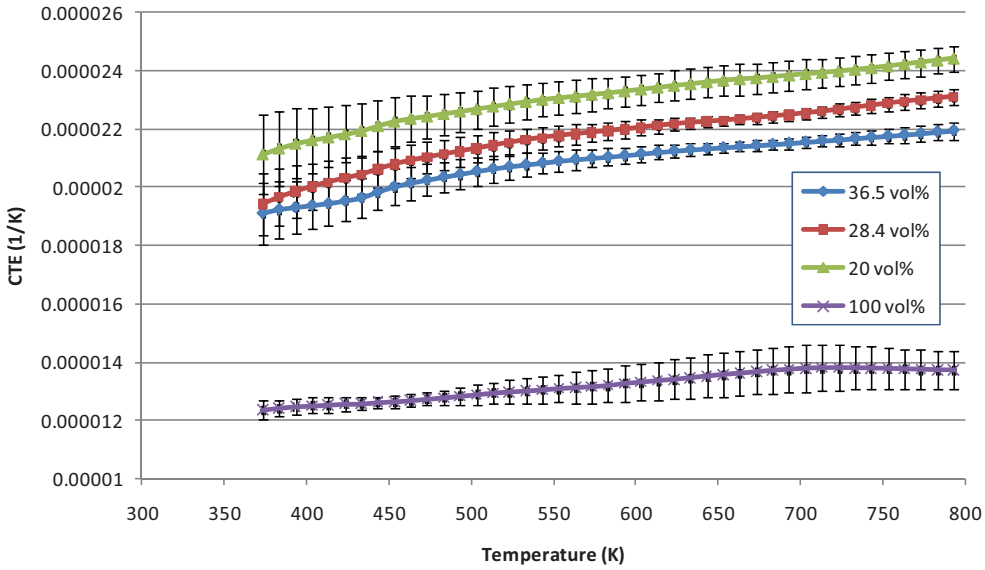

Figure 6 Coefficient of thermal expansion of hafnium aluminide materials.

4. Results

Figure 7 shows a contour plot of temperature distribution of the test assembly under steady-state operation. Table 2 lists the maximum temperatures for the specimen components (those made from the hafnium aluminide materials) for steady-state, two pump operation at nominal cycle power. The maximum component temperature of 462.5 K occurs in the specimen rod in Assembly -1 of the Middle Capsule. Thus, under nominal conditions the specimen temperatures are maintained below 498.2 K, the maximum expected operational temperature of the filter. The maximum predicted specimen temperature is well below the melting temperature of aluminum.

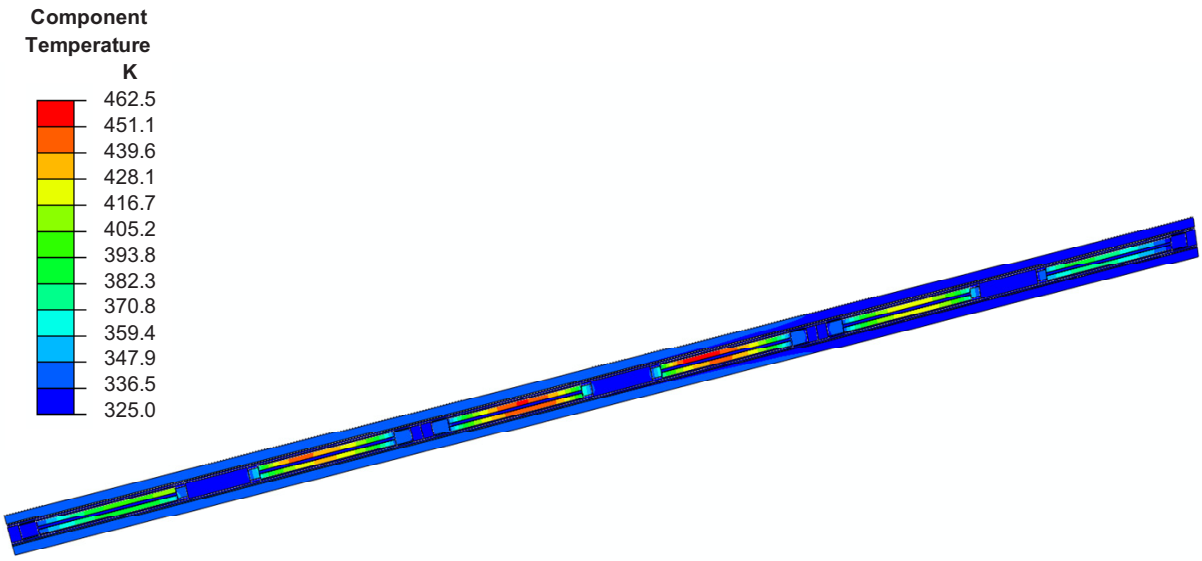

Figure 7. Temperature distribution (K) of the test assembly for steady-state operation at nominal cycle power (24.3 MW(t)).

Table 2. Summary of maximum temperatures for steady-state, two pump operation at nominal cycle power.

Capsule Pair	Assembly	Component	Temperature (K)
A Upper	-1 Top	Flux wire holder	351.9
		Tensile specimens/holder	329.3
		Specimen rods	388.4
	-2 Bottom	Flux wire holder	364.3
		Tensile specimens/holder	340.4
		Specimen rods	424.9
B Middle	-1 Top	Flux wire holder	379.8
		Tensile specimens/holder	341.4
		Specimen rods	462.5
	-2 Bottom	Flux wire holder	379.5
		Tensile specimens/holder	343.2
		Specimen rods	451.7
C Lower	-1 Top	Flux wire holder	371.8
		Tensile specimens/holder	343.0
		Specimen rods	443.6
	-2 Bottom	Flux wire holder	356.1
		Tensile specimens/holder	334.7
		Specimen rods	406.1

5. Summary

Results of thermal hydraulic modeling of an ATR NSUF irradiation experiment performed in conjunction with USU are described. The purpose of the experiment is to determine irradiation-induced changes to a new material designed to function as a thermal neutron filter for fast flux testing of advanced fuels and materials in the ATR. Thermophysical properties of this new material were measured prior to irradiation. After the irradiation campaign is complete, the thermophysical properties of the irradiated specimens will be measured and compared to the preirradiation values. Since thermal neutron flux varies with axial position within the core, the various specimens will be subjected to different heat loads (and temperatures). A finite-element model of the experiment assembly was constructed to predict specimen temperatures during a nominal irradiation cycle. Using finite element analysis, specimen temperatures during irradiation were predicted using a bounding approach to ensure that material temperatures remain below the maximum filter operation temperature. Results from the thermal hydraulic modeling, including the steady-state temperatures of the specimens and capsules, are presented. It was confirmed that all specimen temperatures will be maintained below the maximum filter operating temperature during irradiation. After the irradiation campaign is completed, best-estimate thermal predictions will be performed for the individual specimens using the actual as-run operational power levels and irradiated material properties.

6. Acknowledgment

This work was supported under the auspices of the ATR National Scientific User Facility (NSUF) by the U.S. Department of Energy, Office of Nuclear Energy, under DOE Idaho Operations Office Contract DE-AC07-05ID14517. Arnold Erickson from INL and Kurt Harris from USU fabricated the hafnium aluminide composite material. Professor Heng Ban of USU is the university Principal Investigator on the ATR NSUF project and is responsible for advising the student's research.

7. References

[1] G. R. Longhurst and S. T. Khericha, "Boosted Fast Flux Loop Technical and Functional Requirements," Idaho National Laboratory, 2005.

[2] D. P. Guillen, "Thermal Performance of a Fast Neutron Test Concept for the Advanced Test Reactor," Transactions of the American Nuclear Society and Embedded Topical Meetings, Vol. 98, Anaheim, CA, 2008.

[3] Y. Limoge and A. Barbu, "Amorphization Mechanism in Metallic Crystalline Solids under Irradiation," *Physical Review B,* Vol. 30, Issue 4, 1984, pp. 2212–2215.

[4] L. M. Howe and M. H. Rainville, "A Study of the Irradiation Behavior of Zr_3Al," *Journal of Nuclear Materials,* Vol. 68, 1977, pp. 215–234.

[5] D. P. Guillen "In-Pile Experiment of a New Material to Enable Fast Neutron Testing in ATR," Proceedings of the 2010 International Congress on Advances in Nuclear Power Plants (ICAPP '10), Paper 10115, San Diego, CA, USA, June 13–17, 2010.

[6] H. Wampler, et al., "Fabrication and Characterization of a Conduction Cooled Thermal Neutron Filter," Proceedings of the 2010 International Congress on Advances in Nuclear Power Plants (ICAPP '10), Paper 10118, San Diego, CA, USA, June 13–17, 2010.

[7] Dassault Systèmes Simulia Corp., "ABAQUS/Standard," Version 6.7-3, 2007.

[8] F. P. Incropera and D. P. DeWitt, "Fundamentals of Heat and Mass Transfer," 5th ed., John Wiley & Sons, New York, 2002.

[9] R. H. Perry and D. W. Green, Perry's Chemical Engineers' Handbook, 7th Edition, McGraw-Hill, 1997.

[10] ASTM E1269-05, "Standard Test Method for Determining Specific Heat Capacity by Differential Scanning Calorimetry," ASTM International.

[11] ANSI/ASME Performance Test Codes Standard, PTC 19.1-2005, "Test Uncertainty," The American Society of Mechanical Engineers, 2006.

[12] ASTM B311-08, "Standard Test Method for Density of Powder Metallurgy (PM) Material Containing Less Than Two Percent Porosity," ASTM International, 2008.

[13] ASTM E1461-07, "Standard Test Method for Thermal Diffusivity by the Flash Method," ASTM International, 2007.

[14] B.K. Hodge, and R.P. Taylor, Analysis and Design of Energy Systems, Third Edition, Prentice Hall, New Jersey, 1999, p. 396-419.

[15] S. Min, J. Blumm, and A. Lindemann, "A New Laser Flash System for Measurement of the Thermophysical Properties," *Thermochimica Acta*, Volume 455, Issues 1-2, April 2007, p. 46-49.

[16] J. Blumm, and E. Kaisersberger, "Accurate Measurement of Transformation Energetics and Specific Heat by DSC in the High-Temperature Region," *Journal of Thermal Analysis and Calorimetry*, Vol. 64, 2001, p. 385-391.

[17] ASTM E228-06, "Standard Test Method for Linear Thermal Expansion of Solid Materials with a Push-Rod Dilatometer," ASTM International, 2006.